Non-Stern−Volmer Quenching of S_1 pDFB Fluorescence by O_2 and the Charge Transfer Complex†

Uros S. Tasic, Ernest R. Davidson,‡ and Charles S. Parmenter*

Department of Chemistry, Indiana University, Bloomington, Indiana 47405

Received: October 22, 2002

The vapor phase kinetics of $S_1 \rightarrow S_0$ *p*-difluorobenzene (pDFB) fluorescence quenching by O_2 has been characterized over an O_2 pressure range spanning more than 4 orders of magnitude, ranging from the single-collision regime at less than one Torr to about 37000 Torr. pDFB was pumped to an S_1 level with $\epsilon_{vib} = 3310$ cm^{-1}. Non Stern−Volmer kinetics is observed. The standard Stern−Volmer model, for which the ratio of fluorescence intensity without and with added oxygen against O_2 pressure is linear with an intercept of unity, fits the data only for pressures <10 Torr. At O_2 pressures >3000 Torr, the quenching again becomes linear but with a much lower slope and higher intercept. The quenching rate constants for the low- and high-pressure regimes are 1.3×10^{11} L mol^{-1} $s^{-1} = 7.7 \times 10^6$ $Torr^{-1}$ s^{-1} and 0.13×10^{11} L mol^{-1} $s^{-1} = 0.78 \times 10^6$ $Torr^{-1}$ s^{-1}, respectively. Less detailed studies showed that quenching from S_1 levels with $\epsilon_{vib} = 3705$ and 2887 cm^{-1} has kinetics similar to that of the 3310 cm^{-1} level. A proposed mechanism involving two quenching channels fits the data over the entire pressure range. While there are no data identifying the products of these channels, pDFB T_1 formation may be the rate-determining aspect of the high-pressure quenching. It is suggested that the formation of a pDFB•O_2 charge-transfer complex may be rate controlling at low pressures. Low-level ab initio calculations give a rather tight complex geometry with a ring-to-O_2 distance of 2.5 Å, a dipole moment of 2.6 D, and a net charge transfer of 0.6 electrons. The bonding energy relative to separated $pDFB^+$ and O_2^- was calculated to be 38000 cm^{-1}.

Introduction

Quenching of excited electronic states by interaction with molecular oxygen has been long used as a tool to probe the photophysics and photochemistry of polyatomic molecules.[1] This electronic state destruction is often observed as quenching of $S_1 \rightarrow S_0$ fluorescence and is modeled with the simple Stern−Volmer kinetic scheme. In gas-phase experiments at low pressures of the polyatomic molecule, the only S_1 collisional decay channel will be destruction by the added O_2. If the collisional quenching rate constant is k_q, this scheme leads to the standard Stern−Volmer fluorescence quenching relationship

$$\frac{I_0}{I_M} = 1 + \frac{k_q[O_2]}{k_f}$$

where I_M and I_0 are the fluorescence intensities with and without added O_2 and k_f is the observed rate constant for collision-free fluorescence decay.

O_2 quenching following at least approximately this model has been observed in many studies.[2−5] A Stern−Volmer quenching exploration[6] notable for its extension to unusually high O_2 pressures is found in conjunction with use of $S_1 \rightarrow S_0$ *p*-difluorobenzene (pDFB) fluorescence to explore intramolecular vibrational redistribution (IVR) in the S_1 state. Despite linear Stern−Volmer behavior over the full pressure range, the observed behavior is not strictly that of simple Stern−Volmer kinetics. The intercept is close to five rather than unity as required by the model.

We are using O_2 fluorescence quenching as part of a study of collisional vibrational energy transfer from regions of the vibrational manifold with high state densities.[7] In support of the study, we report here a reinvestigation of O_2 fluorescence quenching kinetics designed to gain an understanding of why deviation from the standard Stern−Volmer model occurs. Quenching of S_1 pDFB fluorescence has been characterized over a pressure range spanning more than 4 orders of magnitude, starting with O_2 pressures below one Torr where, on average, less than one hard-sphere collision occurs during the fluorescence lifetime. Oxygen additions extend to nearly 40000 Torr, roughly the highest pressures used in our earlier study.[6] Monitoring quenching over such a wide range reveals behavior far more complicated than is usually assumed. The simplest kinetic model to account for the observed kinetics involves some sort of reversible product formation in the O_2 interaction. A pDFB•O_2 charge-transfer complex, analogous to others discussed in the oxygen literature,[2,4,8−12] may possess some of the special characteristics required to accommodate the kinetics.

Some of the earlier studies of the interaction of O_2 with aromatic molecules focused on perturbation of singlet−triplet mixing, either theoretically or experimentally in UV absorption spectra.[8−10,13−15] The related phenomenon of excited electronic state quenching by O_2 has been extended to other quenchers such as NO,[16−18] CS_2,[18,19] various ketones, olefins, and even several aromatics.

The scientists honored in this issue of the *Journal of Physical Chemistry* are among the contributors to the literature of

† Part of the special issue "George S. Hammond & Michael Kasha Festschrift".

* Author to whom correspondence should be addressed. Phone: (812) 855-3522. Fax: (812) 855-8300. E-mail: parment@indiana.edu.

‡ Present address: Department of Chemistry, University of Washington, Seattle, WA 98195.

10.1021/jp022281y CCC: $25.00
Published on Web 04/05/2003

quenching and O_2 interactions. George Hammond and his colleagues have published numerous solution quenching studies. One might cite, for example, the diffusion-controlled quenching of an aromatic (a psoralen) by protons[20] or the extraction of Stern−Volmer constants for the fluorescence quenching of phenylated anthracenes by amines.[21] A particularly intriguing example of Michael Kasha's long interest in O_2 interactions with aromatic systems may be found in the development of a new spectroscopic method to observe perturbations of singlet−triplet transitions.[22] Its unique high-pressure application to benzene and pyridine solutions was interpreted in terms of O_2 complexes whose possible geometries in the case of benzene are described with pretty frisky terms, not the least of which is "anf jamel" (Arabic: camel's nose).

Experimental Procedures

The experimental setup for determination of the absolute rate constants for electronic state quenching is similar to that used for studies of IVR in pDFB with high pressures of oxygen.[6,23−25] It consists of a 300 K cross-shaped single-pass stainless steel UV fluorescence cell containing 0.1−0.6 Torr of pDFB to which O_2 is incrementally added. pDFB of 99+% stated purity and extra dry grade O_2 were used. Specific studies established that the gases were well mixed prior to fluorescence measurements. The O_2 pressures varied from slightly less than one Torr corresponding to single-collision conditions for the 5 ns fluorescence lifetime to about 40000 Torr where the collision interval is on the order of a picosecond. Pressures were continuously monitored with MKS Baratron absolute pressure transducers.

pDFB was excited with a 10 Hz Quanta-Ray Nd:YAG pulsed tunable dye laser coupled to a WEX UV wavelength extender. The laser was tuned to pump the pDFB absorption band maximum at 248.98 nm (air), 40152 cm^{-1} (vac).[25] The principal Franck−Condon transition underlying this band reaches the $3^2 5^1$ vibrational level corresponding to an S_1 vibrational energy of 3310 cm^{-1}. We have also extended the study to two other levels.

Fluorescence orthogonal to the laser pump beam was imaged into an 0.85 m spectrometer whose photomultiplier output was read by a gated detection system. The signal was normalized to the laser intensity on a pulse-by-pulse basis. Measuring the electronic quenching involved monitoring the total fluorescence intensity as a function of O_2 pressure. Relative total fluorescence intensities for a series of O_2 pressures were obtained by frequency integrating the spectra. The monochromator was scanned through the spectrum at a relatively low resolution (50−100 cm^{-1}) to give reasonable signal-to-noise while discriminating against scattered light that is an interference particularly prominent at the low fluorescence intensities accompanying high O_2 pressures. It was established that accurate measurements could be acquired by monitoring a central 5000 cm^{-1} segment of the spectrum. A set of measurements usually involved monitoring total fluorescence during six to ten O_2 pressure increments. Many such sets with overlapping O_2 ranges were combined to form the data of this study.

To minimize photochemical degradation, the average laser power was kept relatively low throughout the experiment and the procedure was optimized for minimal pDFB exposure to laser pumping while maintaining an adequate signal-to-noise ratio. Also, the procedure was designed to filter out the different signal intensity contributions that the structured and congested frequency regions of the spectrum have with respect to quenching. Corrections for the background noise and scattered light were made by collecting data from an empty or O_2-filled cell and subtracting this baseline from each scan.

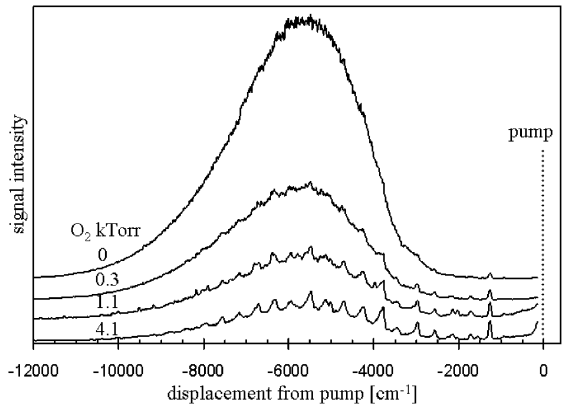

Figure 1. Dispersed fluorescence spectra from the $3^2 5^1$ state of S_1 pDFB (ϵ_{vib} = 3310 cm^{-1}) pumped under collision-free conditions or in the presence of high O_2 pressures. The pump position at 40160 cm^{-1} (the $3_0^2 5_0^1$ absorption maximum) is shown. The spectra are vertically shifted and scaled, but represent qualitatively correct intensity trends. Fluorescence band assignments are given in Figure 4 of ref 6.

Results

As shown in Figure 1, O_2 has two effects on the dispersed fluorescence from the ϵ_{vib} = 3310 cm^{-1} level ($3^2 5^1$). One is transformation of the spectrum from unstructured fluorescence to one with well-developed vibrational bands. This transformation occurs for many other S_1 levels and has been studied extensively as a means to learn about IVR in pDFB.[6,23,25] The second effect is a quenching of fluorescence intensity that accompanies the appearance of vibrational bands. As the pressure of added O_2 climbs above 25 kTorr, the total fluorescence intensity decreases by more than 2 orders of magnitude. The emphasis of the present study concerns the kinetics of this quenching. While simple Stern−Volmer kinetics occurs for the quenching at low O_2 pressures, the data to follow show that the mechanism is far more complicated.

Upon close examination of the spectra in Figure 1, one finds that the intensity in various parts of the spectrum changes at different rates upon O_2 addition, decreasing more rapidly in the central portion than at the edges of the spectrum. It is necessary to integrate the spectrum in order to obtain reliable measurements of total fluorescence intensity. Integration of the central 5000 cm^{-1} region of fluorescence between 32000 and 37000 cm^{-1} provides accurate relative measures of the total intensity. This range includes over 90% of the emission intensity, and it is sufficiently broad to filter out the nonuniformity in the spectral response to O_2 additions.

Figure 2 shows the total fluorescence intensities in the form of the standard Stern−Volmer plot I_0/I_M vs O_2 pressure. The reported pressures in all plots are corrected for nonideal gas behavior using the van der Waals equation and may be directly converted into O_2 concentrations by using the ideal gas law. The plots displayed in Figure 2 show the data of three segments of the complete Stern−Volmer plot. The O_2 pressures for each segment range over about an order of magnitude. Each shows approximate Stern−Volmer behavior with respect to the linearity of the plot, but only for the lowest pressure range (1−10 Torr) do the data have the predicted intercept of one. The intercept is about three and six for the intermediate and highest ranges, respectively. Additionally, the slopes are all different, and the differences far exceed the error bars corresponding to the experimental uncertainty of individual measurements.

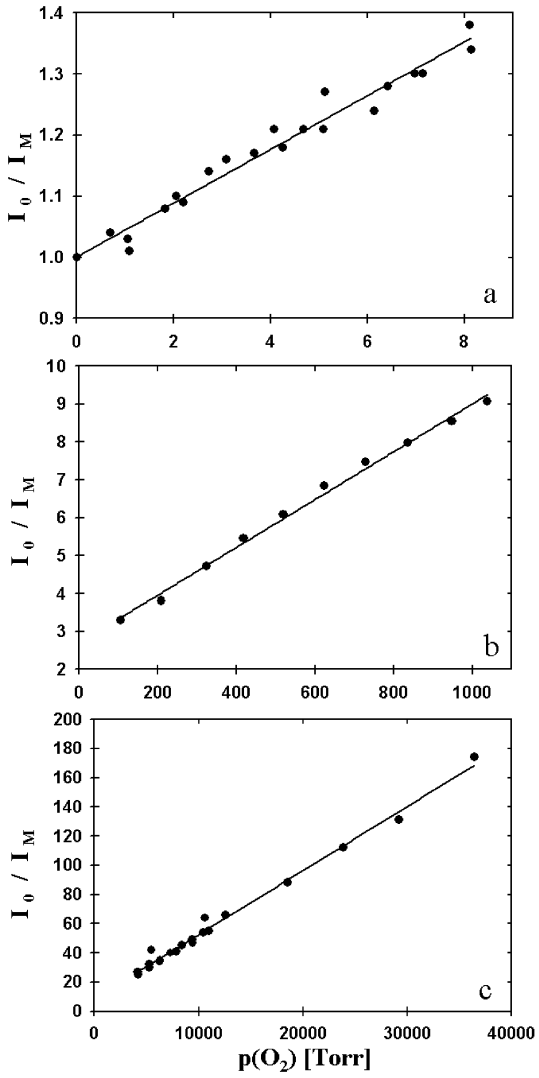

Figure 2. Stern−Volmer plots for quenching of $3^2 5^1$ S_1 pDFB (ϵ_{vib} = 3310 cm^{-1}) fluorescence at (a) low O_2 pressures (1−10 Torr), (b) intermediate pressures (100−1000 Torr), and (c) high pressures (4−40 kTorr). The slopes in 10^{-3} $Torr^{-1}$ of the linear least-squares fits are 44, 6.3, and 4.5 for the low, intermediate, and high-pressure ranges, respectively.

The complete Stern−Volmer plot for the ϵ_{vib} = 3310 cm^{-1} level is displayed in Figure 3. The nonlinearity of the data is evident. The plot is constructed from a series of separate experiments covering five ranges of O_2 pressure, each spanning about an order of magnitude. The initial O_2 pressures were approximately 1, 10, 100, 1000, and 10000 Torr. Each experiment involved six to 10 pressure increments. This degree of detail allowed nonlinearities to be detected with discrimination against random error.

The slopes derived from the lowest- and the highest-pressure data are shown. The low-pressure slope was obtained from three separate sets of measurements using O_2 pressures ranging from one to eight Torr. The high-pressure slope pertains to measurements with O_2 in the range 5000 to 40000 Torr. The limiting slope at low pressure is 44 × 10^{-3} $Torr^{-1}$, and the limiting high-pressure slope is 4.5 × 10^{-3} $Torr^{-1}$. Each was determined from least-squares fits without constraining the intercept to unity. The order of magnitude difference in these slopes emphasizes again the nonlinear nature of fluorescence quenching.

Figure 3 also shows the fluorescence quenching from the ϵ_{vib} = 2887 cm^{-1} level reached by pumping the $3^1_0 5^2_0$ absorption maximum at 251.68 nm (air), 39722 cm^{-1} (vac),[25] and the ϵ_{vib}

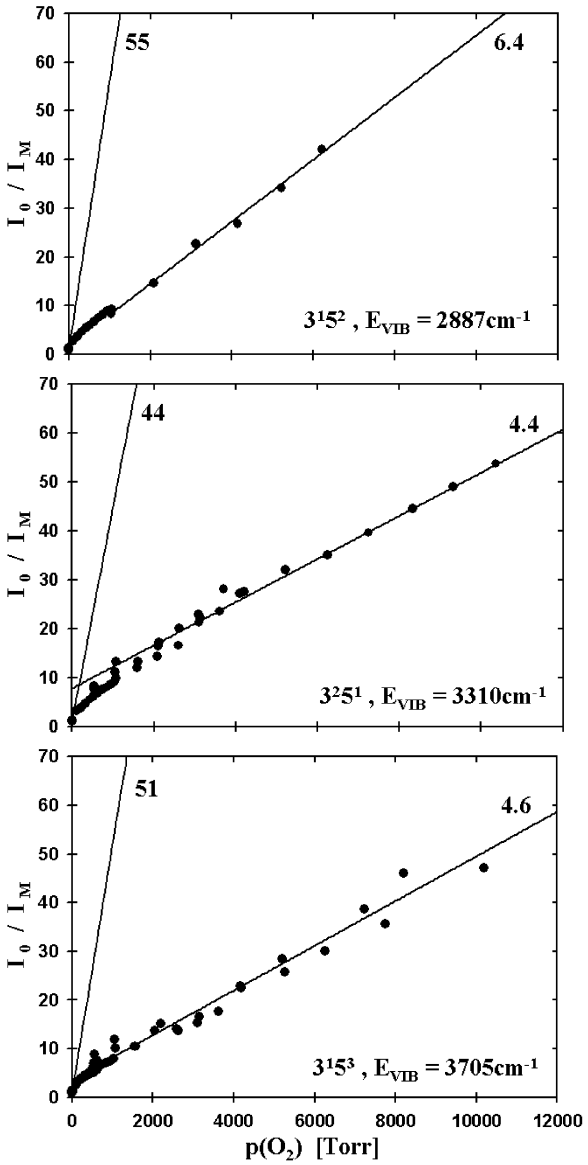

Figure 3. A comparison of Stern−Volmer plots for O_2 quenching of S_1 pDFB fluorescence from the indicted levels. Least squares slopes in 10^{-3} $Torr^{-1}$ for the low (<10 Torr) and high (>2000 Torr) pressure data are shown.

= 3705 cm^{-1} level reached by pumping the $3^1_0 5^3_0$ absorption maximum at 246.64 nm (air), 40533 cm^{-1} (vac). While the studies of these levels are somewhat less detailed, the data establish that the quenching kinetics of both levels match closely those of the 3310 cm^{-1} level described above. The Stern−Volmer plots each have low- and high-pressure regions of linear quenching with a turnover from one region to the other occurring at similar pressures. The limiting low- and high-pressure slopes are indicated in the figure.

The observed deviations from linear Stern−Volmer behavior are negative in the sense that the slope decreases as one goes from low to high O_2 pressures. Several potential experimental artifacts can be eliminated as contributors to the non-Stern−Volmer behavior because they would result in the opposite effect. Reduced pDFB absorption caused by S_0 pDFB destruction from increased complex formation at high O_2 pressures would produce positive deviations. Reduced absorption at high O_2 pressures on account of pressure broadening of the absorption maximum used for laser pumping would have the same effect.

Oxygen-assisted photodegradation of pDFB probably occurs during quenching, and it would also reduce absorption and increase the Stern−Volmer slope. Checks using experiments starting with different O_2 pressures and different pressure ranges yield sets of data that overlap satisfactorily. These tests show that the magnitude of photodecomposition is too small to affect the data.

One might even consider how the extent of pDFB adsorption to the cell wall, i.e., the state of its physisorption equilibrium, could be influenced by added O_2. Through competition for available surface sites, increasing the O_2 pressure at static pDFB pressure reduces the fractional coverage by pDFB, and shifts the dynamic equilibrium for pDFB toward desorption, ultimately resulting in increased gas concentration of pDFB available for pumping. The net effect would be a negative deviation from the linear Stern−Volmer plot. Quenching experiments using different static pDFB pressures suggests that this effect is not significant.

Discussion

The fluorescence quenching data summarized in Figure 3 show that the Stern−Volmer model does not adequately represent the quenching kinetics. Classic Stern−Volmer behavior is observed only for the lowest added O_2 pressures, where the plot of I_0/I_M against O_2 pressure is linear with the required intercept of unity. At much higher pressures, the quenching again becomes linear, but with a substantially different slope and with an intercept well above unity.

The $S_1 \rightarrow S_0$ fluorescence in this study involves appreciable S_1 vibrational excitation. In the present case, $\epsilon_{vib} = 3310\ cm^{-1}$, a value somewhat higher than the $\epsilon_{vib} = 2190\ cm^{-1}$ of our earlier quenching study.[6] It seems unlikely, however, that the limited collisional vibrational relaxation within the S_1 state that competes with the S_1 state destruction is connected to non Stern−Volmer behavior. By using only observations of total fluorescence intensity, our experiments are blind to vibrational energy transfer. Our observations could be affected only if the fluorescence quantum yield from different S_1 vibrational regions varied substantially. Dependence of the fluorescence yield on vibrational energy is small,[26] however, and given that electronic state quenching precludes more than about two vibrational state-changing collisions for an S_1 pDFB molecule, vibrational relaxation cannot be the cause of the special fluorescence quenching behavior.

IVR occurs in the S_1 vibrational regions involved in these O_2 quenching studies. Since fluorescence quantum yield changes are not associated with IVR, our observations of total fluorescence are as blind to this process as they are to collisional vibrational relaxation. Thus, IVR is also an unlikely source of the non Stern−Volmer behavior.

Since we are unable to identify an experimental rationale for the non-Stern−Volmer behavior, it is most likely that the classic Stern−Volmer mechanism does not apply to the quenching of pDFB fluorescence. We note that the observed kinetics occurs also for other S_1 pDFB levels with both higher and lower vibrational energies, as shown in Figure 3. Thus, any revised mechanism would have generality for various areas of the S_1 vibrational manifold.

An Extended Kinetic Model for Oxygen Quenching of S_1 pDFB Fluorescence. The linear behaviors at low and at high O_2 pressures occur with very different Stern−Volmer slopes, so that the quenching is controlled by different channels in these pressure extremes. The most elementary kinetic scheme to accomplish such a channel switch must first involve a collisional channel leading to a dark product such as triplet formation. This irreversible S_1 destruction would be in competition with a second collisional channel leading to a nonemissive product that can reform S_1 pDFB on a subsequent O_2 collision.

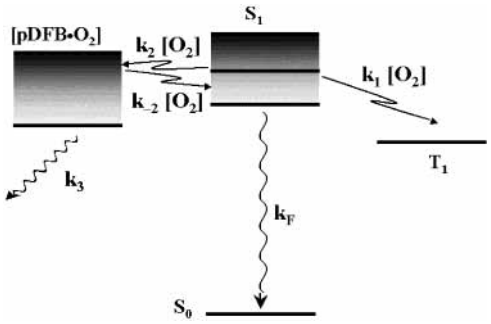

Figure 4. The kinetic mechanism used to account for the quenching of pDFB fluorescence from an excited S_1 vibrational level over the full range of O_2 pressures.

A kinetic mechanism incorporating these concepts is set forth in Figure 4. It is the simplest mechanism that we can devise to account for the data. The following elementary processes define the kinetics following laser excitation of the S_1 state of pDFB.

$$S_1 \xrightarrow{k_f} \text{fluorescence and nonradiative decay} \qquad \text{(A)}$$

$$S_1 + O_2 \xrightarrow{k_1} T_1 + O_2 \qquad \text{(B)}$$

$$S_1 + O_2 \xrightarrow{k_2} [pDFB{\bullet}O_2] \qquad \text{(C)}$$

$$[pDFB{\bullet}O_2] + O_2 \xrightarrow{k_{-2}} S_1 + 2O_2 \qquad \text{(D)}$$

$$[pDFB{\bullet}O_2] \xrightarrow{k_3} \text{nonradiative decay} \qquad \text{(E)}$$

Since the collision-free fluorescence yield is below unity, S_1 pDFB decays by first-order channels that include fluorescence and at least one nonradiative process. The sum of rate constants for these reactions (A) is k_f, and it defines the collision-free fluorescence lifetime $\tau_f = k_f^{-1}$.

With S_1 pDFB + S_0 pDFB collisions precluded by the low pDFB pressure, the only collisional decay channels are those with added O_2. Two such channels must exist. Reaction B involves formation of some nonemitting state that, for convenience, we shall call the pDFB triplet T_1. This dark state may in fact be something else, such as S_0 pDFB or a photochemical intermediate. Whatever the product, the central requirement of reaction B is that it leads to irreversible destruction of S_1 pDFB.

The second collisional O_2 channel, reaction C, must yield a product with two special properties. First, the product must be nonemissive so that reaction C quenches fluorescence, as does reaction B. Second, the product must be able to reform S_1 pDFB with a subsequent O_2 collision. This step is reaction D. The product of reaction C must also decay by a first-order channel represented by reaction E. The essential aspect of this destruction is that it is first-order and that the products are nonemissive. We have proposed in the reaction scheme that the special product involved in reactions C, D, and E is some sort of a complex between pDFB and oxygen, [pDFB•O_2]. We shall discuss below a candidate that might accommodate these special requirements.

These five elementary reactions lead to a pair of coupled linear differential rate equations involving S_1 pDFB and the [pDFB•O_2] complex

$$d[S_1]/dt = -(k_f + k_1[O_2] + k_2[O_2])\,[S_1] + k_{-2}[O_2][\text{pDFB}\bullet O_2]$$

$$d[\text{pDFB}\bullet O_2]/dt = k_2[O_2][S_1] - (k_3 + k_{-2}[O_2])\,[\text{pDFB}\bullet O_2]$$

For a pulsed experiment, these equations yield a solution for the temporal S_1 population with biexponential decay. The solution can then be time-integrated to yield an analytical expression for the relative fluorescence intensity observed with our detection system that integrates the signal produced by each laser pulse. When these relative fluorescence intensities are expressed as the I_0/I_M ratio, one obtains

$$\frac{I_0}{I_M} = 1 + \frac{(k_1k_3 + k_2k_3 + k_1k_{-2}[O_2])[O_2]}{k_f(k_3 + k_{-2}[O_2])} \qquad (1)$$

An equivalent expression may be obtained if we assume continuous wave excitation of S_1 pDFB and use the steady-state assumption $d[\text{pDFB}\bullet O_2]/dt = 0$ for the complex intermediate.

The low-pressure limit of I_0/I_M occurs when $k_{-2}[O_2] \ll k_3$ so that reformation of the S_1 state from the complex intermediate becomes kinetically unimportant.

$$\lim_{[O_2]\to 0} \frac{I_0}{I_M} = 1 + \frac{(k_1 + k_2)[O_2]}{k_f}$$

Alternatively, the high-pressure limit is reached when $k_{-2}\,[O_2] \gg k_3$. At these pressures, the dominant decay channel of the intermediate complex is the collisional reformation of the S_1 state.

$$\lim_{[O_2]\to\infty} \frac{I_0}{I_M} = 1 + \frac{(k_1 + k_2)\,k_3}{k_fk_{-2}} + \frac{k_1\,[O_2]}{k_f}$$

By inspection of these equations, it is seen that the model corresponds at least qualitatively to the observed fluorescence behavior. Linear Stern−Volmer behavior with an intercept of unity is predicted for the lowest O_2 pressures, as observed with data shown in Figure 2a. Linear Stern−Volmer behavior with a different slope and intercept is predicted for high O_2 pressures, as observed with the data shown in Figure 2c. The low-pressure slope is predicted to be greater than that at high pressures, as observed with the data shown in Figure 3. The high-pressure intercept is predicted to be greater than unity, as observed with the data shown in Figure 2c.

The Rate Constants. To analyze the experimental data quantitatively, we recast eq 1 as

$$\frac{I_0}{I_M} = 1 + \frac{(s_0 + s_\infty\alpha[O_2])\,[O_2]}{1 + \alpha[O_2]} \qquad (2)$$

where s_0 and s_∞ are the low- and high-pressure limiting slopes, respectively, given by $s_0 = (k_1 + k_2)/k_f$ and $s_\infty = k_1/k_f$. These slopes are experimentally determined with least-squares fits to the low- and high-pressure data. The remaining parameter $\alpha = k_{-2}/k_3$ is next determined by fitting eq 2 to experimental I_0/I_M data in the intermediate O_2 pressure regime. From s_0 and s_∞, we directly extract the rate constants k_1 and k_2. The α parameter cannot be decomposed into separate values of k_{-2} and k_3. The least-squares fit across the entire O_2 pressure range, spanning more than 4 orders of magnitude, has a standard deviation of ±11%. The rate constants are

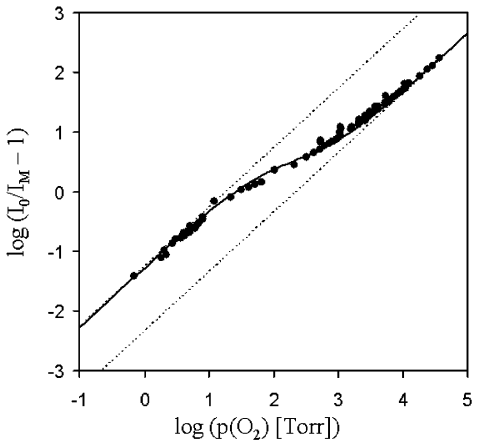

Figure 5. A Stern−Volmer plot of 3^25^1 (ϵ_{vib} = 3310 cm^{-1}) pDFB fluorescence quenching in the unconventional form $\log(I_0/I_M - 1)$ vs $\log(p(O_2))$. Experimental data in addition to those of Figure 2 are used. The full line represents the theoretical fit of the kinetic mechanism as expressed in eq 1. The low and high pressure limit extrapolations are indicated by dotted lines. This representation shows clearly the intrinsic nonlinearity of the quenching, the limiting linear behaviors at the pressure extremes and the quality of the theoretical fit over the full pressure range.

$$k_1 = 1.4 \times 10^{10} \pm 2\%\ \text{L mol}^{-1}\,\text{s}^{-1} = 0.78 \times 10^6\ \text{Torr}^{-1}\,\text{s}^{-1}$$

$$k_2 = 13 \times 10^{10} \pm 4\%\ \text{L mol}^{-1}\,\text{s}^{-1} = 6.9 \times 10^6\ \text{Torr}^{-1}\,\text{s}^{-1}$$

and

$$\alpha = k_{-2}/k_3 = 200 \pm 7\%\ \text{L mol}^{-1} = 0.011\ \text{Torr}^{-1}$$

These values are derived with $k_f = 1.8 \times 10^8\ s^{-1}$ taken from the observed fluorescence lifetime $\tau_f = 5.7$ ns.[27] These constants together completely characterize O_2 quenching of the 3^25^1 S_1 pDFB over a wide pressure range.

The best visual display of the quality of the kinetic fit over the entire O_2 pressure range is provided by the unconventional log−log Stern−Volmer plot in Figure 5. The display also allows one to notice more readily the global changes in the fluorescence quenching kinetics for different O_2 pressures. The two parallel dotted lines each have slope of unity and represent linear extrapolations of the low- and high-pressure limits. The deviation from linearity appears unmistakably in the middle pressure region between about 10 and 3000 Torr. In this range, the two quenching mechanisms occur at competitive rates. Below 10 Torr, the complex formation mechanism dominates the quenching kinetics. Above 3000 Torr, triplet formation dominates the fluorescence quenching. The logs of two limiting slopes can be read from the plot as points where $\log(p(O_2)) = 0$ crosses the upper and lower dotted lines for s_0 and s_∞, respectively. The shift between these two dotted parallel lines is the log of the relative difference between the constants k_1 and k_2. By visual inspection, this shift is about one, reflecting the fact that k_2 is about 10 times larger than k_1.

The Complex. The product of the reversible O_2 collision channel, reaction C, is the central player in the kinetic scheme. What is its identity? This product has two special properties. It must regenerate S_1 pDFB in a subsequent O_2 collision, and it must have a first-order nonradiative decay channel. These

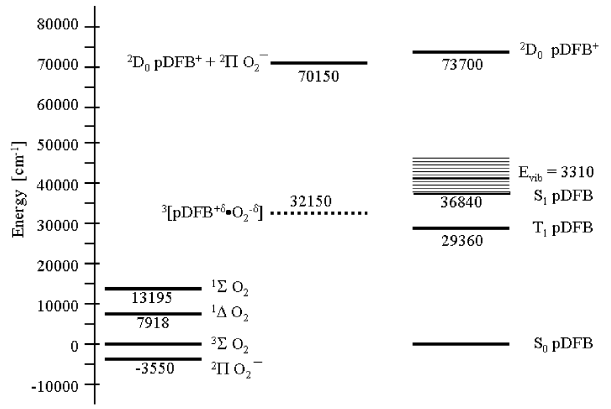

Figure 6. An energy level diagram of a few pDFB and O_2 electronic states relevant to the quenching discussion proposing the participation of a pDFB•O_2 charge-transfer complex. The complex energy is calculated. All others are known experimentally.

constraints probably rule out T_1 and even T_2 pDFB as contenders. While both would be nonemissive and subject to a decay channel, the criterion of reversibility in an O_2 collision would almost certainly be defeated by the high state densities of T_1. The T_2 position is experimentally unknown, but very likely T_2 is strongly coupled to T_1 so that it too would share the T_1 density problem.

Complexes between aromatics and molecular oxygen have been discussed for years in association with excited-state quenching,[2,4,5,11,28] including frequent reference to charge-transfer complexes in particular. Such a complex between O_2 and pDFB is a credible possibility for the product of reaction C. In the absence of experimental information, some of its characteristics may be constructed only with some uncertainties.

An energy level diagram is displayed in Figure 6. The energies of S_1 pDFB[29] and T_1 pDFB,[30−32] the pDFB ionization potential[33,34] to yield the D_0 pDFB$^+$ ion in its zero-point level, the O_2 excited electronic states, and the electron affinity of O_2[35] are all experimentally determined. Those of the charge-transfer complex are calculated.

The pDFB•O_2 complex is a challenge for low-level ab initio quantum chemical methods. The ground triplet state is formed as a van der Waals complex between S_0 pDFB and $^3\Sigma^-_u$ O_2. Second-order perturbation theory (UMP2) using the Gaussian98 program[36] with the 6-31++G** basis set gave a ring-to-O_2 distance of 3.2 Å. Density functional theory (DFT) with the UB3LYP functional is not useful for geometry optimization because this functional does not include the dispersion energy.

Time-dependent DFT (TDDFT) with B3LYP does provide a crude estimate of the excited states of pDFB. This gives the vertical energy of the T_1 state to be 30400 cm^{-1}. With both TDDFT and single excitation configuration interaction (CIS), this state is predicted to be of B_{1u} symmetry and is a mixture of $a_u \leftarrow b_{1g}$ and $b_{3u} \leftarrow b_{2g}$ excitations. By contrast, T_2 at 33000cm^{-1} is the HOMO−LUMO $a_u \leftarrow b_{2g}$ excitation with B_{2u} symmetry. While these energies are in fair agreement with the known T_1 energy of pDFB, the corresponding S_1 energy is too high. TDDFT predicts S_1 to be the HOMO−LUMO $a_u \leftarrow b_{2g}$ B_{2u} excited state at about 41200 cm^{-1} vertically.

The O_2 molecule can form weak van der Waals complexes with each of these pDFB states to form states with total spin of 1. Additionally, the low-energy singlet excited states of O_2 can couple to the pDFB triplet states to form additional triplet states. The lowest three singlet states of the complex are formed from the singlet excited states of O_2 combined with the S_0 state of pDFB. Excited singlet states can be formed from a complex of ground triplet state O_2 with T_1-excited pDFB.

Another set of states can be formed as charge-transfer complexes. The ground D_0 state of the pDFB cation can form a complex with the ground $^2\Pi$ state of the O_2 anion. This combination can make two singlet and two triplet states. Geometry optimization or energy calculations on most of these states is not feasible because there are several lower states of the same symmetry with which they will mix. For example, if the O_2 is parallel to the C−F bond axes with the z axis chosen perpendicular to the pDFB plane, then the charge-transfer complex with the O_2 π_z^* orbital doubly occupied has the same symmetry as the ground T_0 state of the complex. Mixing with the ground state then stabilizes the T_0 state but destabilizes the charge-transfer state. This mixing is even stronger in other cases where the energy difference is small. The charge-transfer triplet state formed with π_z^* singly occupied has the same symmetry as the complex between S_1 and O_2 or between T_2 and O_2. The singlet CT complexes similarly can mix with the T + O_2 singlet states.

With the O_2 axis turned to be orthogonal to the C−F bond axes, the triplet CT complex with π_z^* doubly occupied is lower in energy than any other state of this symmetry so that a calculation was possible. With this orientation, B3LYP geometry optimization gave a rather tight complex with a ring-to-O_2 distance of 2.5 Å. The bonding energy relative to pDFB$^+$ and O_2^- was calculated to be 38000 cm^{-1} compared to the interaction energy of point charges at this distance of 46000 cm^{-1}. This complex was computed to have a dipole moment of 2.6 D and a net charge transfer of 0.6 electrons.

Since the complex characteristics are not well-defined, one can explore only the plausibility of meeting the kinetic model requirements. We first note that complexes with predominantly charge transfer character are likely to be nonemissive. The transition matrix element for emission is small since it is approximately between an orbital localized on O_2 and an orbital localized on pDFB. The collision-free decay channel (reaction E) concerns internal conversion or intersystem crossing resulting from coupling among complex states to produce a state with low probability of reforming S_1 pDFB on a subsequent O_2 collision. The complex shown in Figure 6 will be formed with substantial vibrational energy. This energy reduces the energetic challenges in the collisional dissociation of the complex to reform S_1 pDFB. According to the energetics presented in Figure 6, the rate constant k_{-2} for this dissociation should be large, approaching that of a hard-sphere collision, to minimize collisional vibrational energy loss in the complex prior to the collision that leads to dissociation. Unfortunately, we cannot measure k_{-2} in our experiments.

Conclusion

Kinetics of O_2 fluorescence quenching has been reinvestigated in an attempt to gain understanding of why deviation from the standard Stern−Volmer model occurs. Quenching has been characterized over a pressure range spanning almost 5 orders of magnitude, starting with O_2 pressures near one Torr where, on average, less than one hard-sphere collision occurs during the fluorescence lifetime. Monitoring quenching over this wide range reveals two distinct pressure regimes of pseudo Stern−Volmer behavior. The simplest kinetic model that seems to account for the observed behavior involves a simple irreversible collisional decay channel plus a second collisional channel that makes a nonemissive product with a special characteristic. A subsequent O_2 collision with the product reforms S_1 pDFB. A

pDFB•O_2 charge-transfer complex might possess the requirements of this product. At low O_2 pressures, the quenching rate is controlled by the formation of this reversible product. At high O_2 pressures, the kinetic control of quenching switches to the irreversible channel.

Some of the characteristics of a pDFB•O_2 charge-transfer complex emerge from ab initio calculations. With a net charge of 0.6 electrons and a rather tight geometry, its energy, as shown in Figure 6, is near that of S_1 pDFB.

Acknowledgment. This work was supported by Grants No. CHE-9982415 and CHE-9910430 from the National Science Foundation. Earlier work on O_2 quenching of fluorescence from various S_1 pDFB vibrational levels by Drs. D. L. Catlett and T. A. Stone has been most helpful. We appreciate the skills and availability of Mr. Larry Wolford who was a principal factor in maintaining laser function during these studies.

References and Notes

(1) Turro, N. J. *Modern Molecular Photochemistry*; University Science Books: Mill Valley, CA, 1991.

(2) Brown, R. G.; Phillips, D. *J. Chem. Soc. Faraday Trans. II* **1974**, *70*, 630.

(3) Kikuchi, K. *Chem. Phys. Lett.* **1991**, *183*, 103.

(4) Kikuchi, K.; Sato, C.; Watabe, M.; Ikeda, H.; Takahashi, Y.; Miyashi, T. *J. Am. Chem. Soc.* **1993**, *115*, 5180.

(5) Grewer, C.; Brauer, H. D. *J. Phys. Chem.* **1994**, *98*, 4230.

(6) Coveleskie, R. A.; Dolson, D. A.; Parmenter, C. S. *J. Phys. Chem.* **1985**, *89*, 645.

(7) Stone, T. A.; Parmenter, C. S. *J. Phys. Chem. A* **2002**, *106*, 938.

(8) Murrell, J. N. *Mol. Phys.* **1960**, *3*, 319.

(9) Tsubomura, H.; Mulliken, R. S. *J. Am. Chem. Soc.* **1960**, *82*, 5966.

(10) Lim, E. C.; Kowalski, V. L. *J. Chem. Phys.* **1962**, *36*, 1729.

(11) Sato, C.; Kikuchi, K.; Okamura, K.; Takahashi, Y.; Miyashi, T. *J. Phys. Chem.* **1995**, *99*, 16925.

(12) Birks, J. B.; Pantos, E.; Hamilton, T. D. S. *Chem. Phys Lett.* **1973**, *20*, 544.

(13) Evans, D. F. *J. Chem. Soc.* **1957**, 1351.

(14) Evans, D. F. *J. Chem. Soc.* **1957**, 3885.

(15) Evans, D. F. *J. Chem. Soc.* **1959**, 2753.

(16) Brown, R. G.; Phillips, D. *J. Chem. Soc., Faraday Trans. 2* **1974**, *70*, 1435.

(17) Chihara, K.; Baba, H. *Chem. Phys.* **1977**, *25*, 299.

(18) Coveleskie, R. A.; Dolson, D. A.; Moss, D. B.; Munchak, S. C.; Parmenter, C. S. *Chem. Phys.* **1985**, *96*, 191.

(19) Groenzin, H.; Mullins, O. C.; Mullins, W. W. *J. Phys. Chem. A* **1999**, *103*, 1504.

(20) Menger, E. L.; Bhattacharjee, H. R.; Hammond, G. S. *Photochemistry and Photobiology* **1979**, *29*, 393.

(21) Lishan, D. G.; Hammond, G. S.; Yee, W. A. *J. Phys. Chem.* **1981**, *85*, 3435.

(22) Khalil, G. E.; Kasha, M. *Photochem. Photobiol.* **1978**, *28*, 435.

(23) Coveleskie, R. A.; Dolson, D. A.; Parmenter, C. S. *J. Phys. Chem.* **1985**, *89*, 655.

(24) Holtzclaw, K. W.; Parmenter, C. S. *J. Phys. Chem.* **1984**, *88*, 3182.

(25) Holtzclaw, K. W.; Parmenter, C. S. *J. Chem. Phys.* **1986**, *84*, 1099.

(26) Volk, L. J.; Lee, E. K. C. *J. Chem. Phys.* **1977**, *67*, 236.

(27) Guttman, C.; Rice, S. A. *J. Chem. Phys.* **1974**, *61*, 661.

(28) Kearns, D. R.; Stone, A. J. *J. Chem. Phys.* **1971**, *55*, 3383.

(29) Coveleskie, R. A.; Parmenter, C. S. *J. Mol. Spectrosc.* **1981**, *86*, 86.

(30) Metcalfe, J.; Rockley, M. G.; Phillips, D. *J. Chem. Soc., Faraday Trans. 2* **1974**, *70*,1660.

(31) Childs, A. F.; Dunn, T. M.; Francis, A. H. *J. Mol. Spectrosc.* **1983**, *102*, 56.

(32) Swiderek, P.; Schurfeld, S.; Winterling, H. *Ber. Bunsen-Ges. Phys. Chem.* **1997**, *101*, 1517.

(33) Sekreta, E.; Viswanathan, K. S.; Reilly, J. P. *J. Chem. Phys.* **1989**, *90*, 5349.

(34) Fujii, M.; Kakinuma, T.; Mikami, N.; Ito, M. *Chem. Phys. Lett.* **1986**, *127*, 297.

(35) Herzberg, G.; Huber, K. P. *Molecular Spectra and Molecular Structure IV. Constants of Diatomic Molecules*; Van Nostrand Reinhold Co.: New York, 1979.

(36) Frisch, M. J.; Trucks, G. W.; Schlegel, H. B.; Scuseria, G. E.; Robb, M. A.; Cheeseman, J. R.; Zakrzewski, V. G.; Montgomery, J. A., Jr.; Stratmann, R. E.; Burant, J. C.; Dapprich, S.; Millam, J. M.; Daniels, A. D.; Kudin, K. N.; Strain, M. C.; Farkas, O.; Tomasi, J.; Barone, V.; Cossi, M.; Cammi, R.; Mennucci, B.; Pomelli, C.; Adamo, C.; Clifford, S.; Ochterski, J.; Petersson, G. A.; Ayala, P. Y.; Cui, Q.; Morokuma, K.; Malick, D. K.; Rabuck, A. D.; Raghavachari, K.; Foresman, J. B.; Cioslowski, J.; Ortiz, J. V.; Baboul, A. G.; Stefanov, B. B.; Liu, G.; Liashenko, A.; Piskorz, P.; Komaromi, I.; Gomperts, R.; Martin, R. L.; Fox, D. J.; Keith, T.; Al-Laham, M. A.; Peng, C. Y.; Nanayakkara, A.; Gonzalez, C.; Challacombe, P. M.; Gill, M. W.; Johnson, B. G.; Chen, W.; Wong, M. W.; Andres, J. L.; Head-Gordon, M.; Replogle, E. S.; Pople, J. A. *Gaussian 98* (Revision A.7); Gaussian, Inc.: Pittsburgh, PA, 1998.